International Journal of Energy Research

INTERNATIONAL JOURNAL OF ENERGY RESEARCH
Int. J. Energy Res. (2014)
Published online in Wiley Online Library (wileyonlinelibrary.com). DOI: 10.1002/er.3238

Efficiency assessment for a small heliostat solar concentration plant

M. Renzi[1,*,†], C. M. Bartolini[2], M. Santolini[3] and A. Arteconi[2]

[1]Facoltà di Scienze e Tecnologie, Libera Università di Bolzano, Piazza Università 5 39100 Bolzano, Italy
[2]Università degli Studi e-Campus, Via Isimbardi, 10 22060 Novedrate CO, Italy
[3]Dipartimento di Energetica, Università Politecnica delle Marche, Via Brecce Bianche, 1 60131 Ancona Italy

SUMMARY

In this paper, a small non-imaging focusing heliostat is presented, and an analytical model for assessing its performance is described. The main novelty of the system lies in the tracking mechanism and the mirror mount, which are based on off-the-shelf components and allow a good trade-off between accuracy and costs. The concentrator mirrors are moved by this two-axis tracking machinery to reflect the sun's rays onto a fixed target, the dimensions of which can be varied to suit the user's needs. A prototype plant to be located in central Italy was designed and simulated with a ray-tracing algorithm, and it comprises 90 heliostats for a total reflective area of 7.5 m^2. The reflected solar rays are tracked taking the mechanical positioning errors of the tracking system into account. The total flux of radiation energy hitting the target was determined, and intensity distribution maps were drawn. Simulations showed that the system's optical efficiency can exceed 90% in summer, despite the tracking errors, mainly because of the smaller distance between the heliostats and the receiver. The solar concentration ratio over a receiver of 250 mm in diameter reached 80 suns with a very good uniformity. Over a 400-mm receiver, the concentrated radiation was less uniform, and the solar concentration ratio reached 50 suns, with a higher optical efficiency and collected solar radiation. The present concentration ratio is still suitable for many applications ranging from the electric power production, industrial process heat, and solar cooling. Copyright © 2014 John Wiley & Sons, Ltd.

KEY WORDS

heliostat; solar concentration; CSP; flat mirrors; small scale

Correspondence

*M. Renzi, Facoltà di Scienze e Tecnologie, Libera Università di Bolzano, Piazza Università 5 39100 Bolzano, Italy.
†E-mail: massimiliano.renzi@unibz.it

Received 16 December 2013; Revised 16 June 2014; Accepted 18 June 2014

1. INTRODUCTION

Concentrated solar power (CSP) is a term describing a technology for concentrating sunlight from a large area onto a small area by means of lenses or mirrors. The concentrated light is typically converted into electrical power or can be used as a thermal energy source. CSP is considered a potential alternative to power generation from fossil-fueled power plants because it has a lower environmental impact, mitigating carbon emissions [1–3]; in the short term, the hybridization of traditional plants is foreseen as the most viable solution [4].

Although present-day CSP plants are generally large solar farms between 50 and 280 MW in size [5], there is increasing interest in medium-scale and small-scale applications. An interesting study by Rawlins and Ashcroft [6] highlights, for example, the potential of small CSP systems in emerging countries (the MENA region, South Africa, central and south America) for industrial heat and rural off-grid applications. Medium-sized CSP plants currently represent a niche market. They can fuel remote facilities (such as mines and cement factories) or produce industrial process heat. Small CSP devices (typically coupled with organic Rankine cycles, microturbines, or Stirling engines) can be used, instead, on the roofs of buildings to provide electricity, heating and cooling, or daylight [7–11], thanks to their small size that allows a flexible installation of the concentrator and the receiver.

Medium-sized and small-sized CSP plants will become a viable solution if the related costs can be contained, and this demands significant research and development efforts concerning the mirrors, heliostats, focus receivers, and power blocks [2]. Scaling down generally has little economic appeal because of the high cost of the tracking mechanism. To achieve good techno-economic results, the cost of the tracking system would need to be reduced without loss of tracking accuracy.

This work concerns a non-imaging focusing heliostat consisting of arrays of many small movable mirrors. Interesting studies by Chen *et al*. [12–15] and Chong [16] have dealt with non-imaging focusing heliostats, showing design and construction procedures for CSP plants intended for various applications, such as photovoltaic (PV) panels, food processing, and high-temperature solar furnaces. In particular, Chen *et al*. [13] developed a solar concentrator with two tracking systems. A matrix of 25 flat mirrors, moved as a single heliostat, is mounted on the primary tracker. Then all the mirrors are moved by a secondary moving system that corrects the position of each mirror to approximate a parabolic shape, thus reducing the aberration effect and optimizing the concentration ratio. By adding a secondary parabolic concentrator, this system can achieve very high concentration ratios, and a maximum temperature of 3400 °C was recorded. Subsequently, the concentrator was redesigned in order to reduce its realization costs for the application in food processing [15]. Chong *et al*. [16,17] proposed a solution to scale down the cost of a $105 \times 105\,cm^2$ focusing heliostat still achieving very high concentration ratios over 1000 suns.

The object of this paper is to present a small CSP unit in which small-sized heliostats are used to focus the light on the receiver and each heliostat is moved independently by a couple of stepper motors: the frame where the heliostats are mounted is fixed, while each single heliostat is moved. The weight of each element is thus reduced, and there is no need for major building works or cumbersome trackers; only a sufficiently rigid structure is required. The tracking mechanism is based on off-the-shelf components and allows a good trade-off between accuracy and costs. The concentration ratio, the total power, and the size of the focal spot can be adjusted as a function of the size and number of the heliostats.

The optical efficiency of such a system can be very high because the distance of the heliostats from the focal point is small and the optical losses can be limited. This issue was also studied by Danielli *et al*. [18], who described a tower plant having several heliostats' micro-fields with an independent tower receiver each. Being the packing factor 46%, their average annual optical efficiency is about 87%, without taking into account shadowing losses, blocking losses, and heliostats' tracking errors. High optical performance is achieved, thanks to the very low distance-to-tower-height ratio of the heliostats, which ranges between 2.6 and 4.3 for the furthermost heliostat in the studied configurations. It is demonstrated that this parameter is one of the most important to optimize the optical efficiency of a central receiver concentration plant. Another similar study on the same topic was published by Schramek and Mills [19] who proposed a multi-tower solar array configuration with dynamic receiver allocation. This solution improves the ground usage and reduces the inefficiency of the widely spaced remote heliostats of a large tower system. In addition, the reduced distance of the heliostats from the focal point ensures the minimization of astigmatism and aberrations.

The small-sized heliostat concentrator described here was analyzed with an analytical simulation model based on ray-tracing algorithms with an objective to demonstrating that the system could achieve a good overall optical efficiency even if off-the-shelf components for the tracking system with relatively low accuracy are used. Possible applications for such a system are described.

2. SMALL-SIZED HELIOSTAT CONCENTRATOR

A non-imaging heliostat concentrator is designed with a view to achieving a good optical efficiency with a reasonably high concentration ratio on the target. This concentrator consists of numerous hexagonal flat mirrors acting as an optical element to collect and focus incident light on a target.

The following sections describe the basic principles behind the concentrator operation and the concentrator design.

2.1. Basic principles behind the concentrator

In a heliostat concentrator, the sunlight is concentrated by superposing the reflected images from a number of flat mirrors on a single target [20]. In our system, the incident solar rays are reflected onto the target by arrays of identical hexagonal flat mirrors in order to obtain a uniform intensity and medium concentration ratio (Figure 1). The hexagonal shape was adopted to achieve a more efficient use of the space with a better packing of the heliostats and with a reduced blocking and shadowing effect, as further explained in Section 2.2. An algorithm was developed to simulate the concentrator's performance. This algorithm can be adjusted for any mirror position once the desired distribution was defined. The first step involved defining the system of coordinates, the origin of which was placed on a flat surface at the bottom left-hand corner of the concentrator: the x-axis was directed toward the east cardinal point, the y-axis toward the north, and the z-axis toward the zenith.

The focusing heliostat concentrator can be seen as consisting of $n \times m$ mirrors. The position of each mirror in the concentrator can be indexed as (i, j), where i and j indicate the mirror located in i-th row and j-th column of the concentrator. The concentrator's odd-numbered columns are offset with respect to the even-numbered columns by half the pace of a mirror. This helps to reduce the shadowing and blocking effect during the early and late hours of the day. The coordinate of the central point for the corresponding i,j-mirror, $P_{i,j}$, can be written as follows:

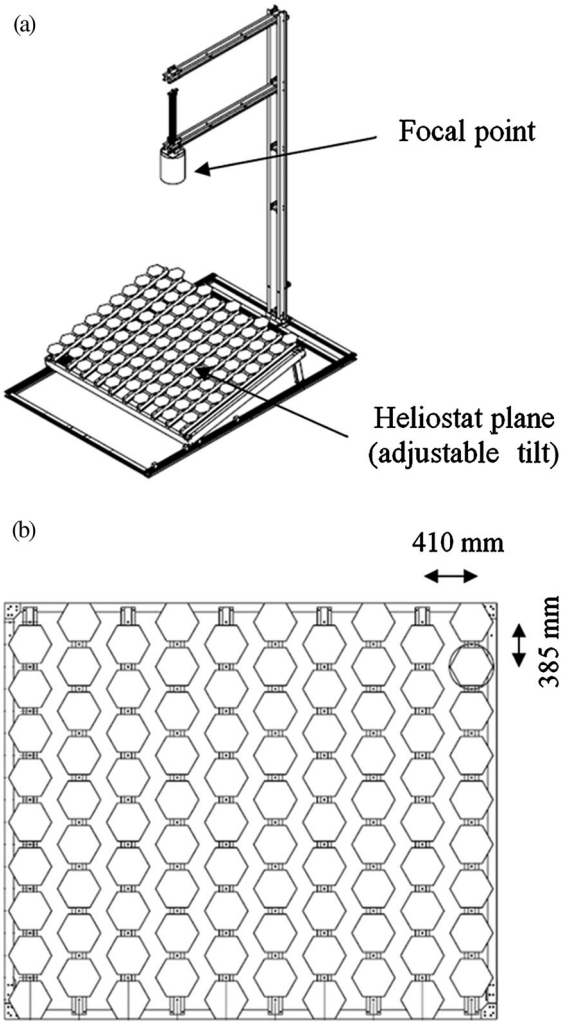

Figure 1. (a) Small-sized hexagonal heliostat plant and (b) heliostats distribution (plan view).

$$P_{ij} = \begin{bmatrix} x_{P,ij} \\ y_{P,ij} \\ z_{P,ij} \end{bmatrix}_{ij} = \begin{bmatrix} \frac{1}{2} + \left(l + d_{j,j+1}\right)\cdot(i-1) \\ \left(h + d_{i,i+1}\right)\cdot(m-y) + \left(h + d_{i,i+1}\right)/2\cdot(1-res) \\ hz \end{bmatrix}_{ij} \quad (1)$$

where l is the diagonal of the mirror, h is the height of the hexagon, $d_{i,i+1}$ is the distance between two mirrors in adjacent rows, $d_{j,j+1}$ is the distance between two mirrors in adjacent columns, m is the number of columns, hz is the height of the mirror off the ground, and res is a parameter that shifts the odd-numbered columns northward to take the correct position of the center of each mirror into account, that is, $res = 1$ for the even-numbered columns, while $res = 0$ for the odd-numbered columns.

If necessary, the plane on which the heliostat lies can be rotated around the x-axis to reduce the shadow effect and improve the concentrator's performance. If the angle of rotation is φ, the rotated position of the center of the mirror is as follows:

$$Pr_{ij} = \begin{bmatrix} x_{p,ij} \\ y_{p,ij} \\ z_{p,ij} \end{bmatrix}_{ij} = \begin{bmatrix} x_{P,ij} \\ y_{P,ij}\cos(\varphi) - Z_{P,ij}\sin(\varphi) \\ z_{P,ij}\sin(\varphi) - Z_{P,ij}\cos(\varphi) \end{bmatrix}_{ij} \quad (2)$$

The coordinates of the focus (receiver) can be set by the user according to need, and they can generally be written as follows:

$$F = \begin{vmatrix} x_F \\ y_F \\ z_F \end{vmatrix} \quad (3)$$

Given these points, the distance of each mirror from the focal point d_{F_Pr} can be calculated as follows:

$$d_{F-Pr,ij} = \sqrt{\left(x_F - x_{Pr,ij}\right)^2 + \left(y_F - y_{Pr,ij}\right)^2 + \left(z_F - z_{Pr,ij}\right)^2} \quad (4)$$

The unit vector pointing from the mirror to the receiver can be calculated as follows:

$$\overrightarrow{r_{ij}} = \begin{bmatrix} r_{x,ij} \\ r_{y,ij} \\ r_{z,ij} \end{bmatrix}_{ij} = \begin{bmatrix} \left(x_F - x_{Pr,ij}\right)/d_{F-Pr,ij} \\ \left(y_F - y_{Pr,ij}\right)/d_{F-Pr,ij} \\ \left(z_F - z_{Pr,ij}\right)/d_{F-Pr,ij} \end{bmatrix}_{ij} \quad (5)$$

The other information needed to calculate the reflection of the solar radiation from each mirror onto the target is the sun's position in the sky. Several authors have developed algorithms to calculate the sun azimuth and zenith angles, and many studies have emphasized how important it is to establish the sun's position precisely to achieve better concentration performance [21]. Michalsky's formulation was used in our work [22], because this algorithm offers a good trade-off between precision and computational requirements.

The components of the unit vector representing the direction of the sun's rays are as follows:

$$\overrightarrow{s_{ij}} = \begin{bmatrix} s_{x,ij} \\ s_{y,ij} \\ s_{z,ij} \end{bmatrix}_{ij} = \begin{bmatrix} cos(\theta_s)sin(\alpha_s) \\ cos(\theta_s)cos(\alpha_s) \\ sin(\alpha_s) \end{bmatrix}_{ij} \quad (6)$$

where θ_s is the elevation angle and α_s is the azimuth angle according to Michalsky's algorithm.

The principle governing the displacement of heliostat mirrors to reflect solar radiation onto a focal point is that the normal vector to the mirror should always be the bisector of the sunbeam and the reflected ray vectors. The normal vector $\overrightarrow{N_{ij}}$ is defined as the sum of the sunbeam

and the mirror-to-receiver vector:

$$\overrightarrow{N_{ij}} = \vec{s}_{ij} + \vec{r}_{ij} \tag{7}$$

and the corresponding unit vector $\overrightarrow{n_{ij}}$ is as follows:

$$\overrightarrow{n_{ij}} = \begin{bmatrix} n_{x,ij} \\ n_{y,ij} \\ n_{z,ij} \end{bmatrix}_{ij} = \begin{bmatrix} N_{x,ij}/\left|\vec{N}\right| \\ N_{y,ij}/\left|\vec{N}\right| \\ N_{z,ij}/\left|\vec{N}\right| \end{bmatrix}_{ij} \tag{8}$$

The bisector $\overrightarrow{n_{ij}}$ vector is calculated for each mirror and transformed from a Cartesian vector into a spherical coordinate system to obtain the tracking elevation angle θ_{ij},

$$\theta_{ij} = 90 - atan2\left(n_{z,ij}, \sqrt{n_{x,ij}^2 + n_{y,ij}^2}\right) \tag{9}$$

and the tracking azimuth angle α_{ij},

$$\alpha_{ij} = -atan2\left(n_{y,ij}, n_{x,ij}\right) - 90. \tag{10}$$

The motors moving the mirrors are stepper motors. The tracking system is an azimuth-elevation mechanism, mounted under each heliostat. The azimuth motor shaft is mounted on a chassis so that the axis of motion is perpendicular to the mirror's plane. The zenith motor shaft has its axis of motion parallel to the ground. The azimuth shaft's tracking is barycentric, while the zenith shaft's axis is 48 mm away from the mirror's center of mass. Because the moving mechanism in the prototype plant is not fully barycentric, an iterative algorithm was implemented to correct the bisector vector, $\vec{N}$. The mirrors start to move from a well-known zero position (azimuth = −90° counterclockwise from the south; zenith: 0°), and the stepper motors move until they reach the angle required. A printed circuit board and an electronic routing device indicate the number of steps that each stepper motor has to move. A detailed description of the electronic controller of the presented solar concentrator can be found in [23].

2.2. Concentrator design

The concentrator was planned for small-scale applications (max collected power 6 kW) and to be installed in a town of central Italy (local coordinates: 43°35′55.82″N and 13°20′50.02″E). Thus, the design presented in this work comprises 90 hexagonal heliostats placed over a structure consisting of 10 steel columns forming a rigid frame and ensuring the necessary mounting accuracy. This structure is mounted on a chassis with an inclination that can be adjusted. Its axis of rotation is parallel to the *x*-axis of the system of coordinates described in the previous section. The heliostat plane can also slide along the *y*-axis over a total stroke of 2000 mm (Figure 1). The position of the receiver can be adjusted in order to avoid any shadowing effect on the heliostats when the sun reaches the highest elevation. The *y*-axis can be aligned over the north–south axis by calculating the local mid-day time at the site of the concentrator's installation. The sides of the hexagonal mirrors are 180 mm long, and the total reflecting surface area of the 90 mirrors is 7.5 m^2. Each mirror is supported by a proper tracking mechanism. The overall weight of the mechanism, the mirror mount, and the mirror itself is about 0.71 kg, meaning that the weight of the heliostat per reflective area is 8.5 kg/m^2, which is a very low value if compared with large-scale systems, whose weight generally ranges between 30 and 40 kg/m^2, even if there are some ongoing research projects that aim at reducing the weight of the heliostats to 15–20 kg/m^2 in order to reduce the cost of the plant [24].

The system is designed so that the focal point can be set at different distances from the ground, from a height of 2500 mm up to 5000 mm above ground level, covering a total stroke of 2500 mm. The position of the concentrator's focus on the *x*-axis is fixed and centered over the concentrator's mid-point.

The distance between the central points of two adjacent heliostats on the same column is 385 mm, and on adjacent columns, it is 410 mm (Figure 1). Some studies [25,26] investigated the ideal heliostat layout for the optimal performance of solar tower plants. These papers describe the optimal layout of the solar field to optimize the packing factor with a minimal decay of the optical efficiency: a packing factor (ratio of the reflective area and the overall space occupancy) in the range of 30% is a typical value for a large heliostat plant. In our case, however, the heliostat layout is designed to obtain a compact system with reasonable blocking and shadowing losses. Because the distance of the heliostats from the receiver is always smaller than the height of the tower, it is still possible to achieve a good optical efficiency with limited blocking and shadowing losses even with a higher packing factor, as reported in a recent paper [27]. The design packing factor of the presented concentrator is about 50%, which is a high but reasonable value for the heliostats installed close to the receiver. In addition, the use of a tilted mounting surface for the heliostats can further reduce the shadowing losses as will be described hereinafter in the results section.

Each heliostat is moved by two stepper motors. These motors were chosen to enable a good tracking performance with an adequate moving and holding torque. As explained previously, the first motor is used to track the azimuthal movement of the sun, the second to track the elevation apparent motion of the sun. Both the stepper motors use a high gear reduction ratio, totaling 1500:1, which is needed to obtain enough torque from the motors to move the whole heliostat and avoid any unwanted heliostat movement under external forces (detent torque), such as that of the weight of the heliostat, or the aerodynamic force of the wind, and so on. The low weight of the heliostats is a key factor that makes possible to adopt very small and low cost tracking engines. The reduction gear enables very accurate heliostat positioning and torque: the resolution in the rotary motion is 0.005°, the moving torque is 5.0 Nm, and the detent torque 7.1 Nm. Because this system was

assembled using readily available (off-the-shelf) and reasonably priced components, it is quick and easy to implement. The stepper motors require a 24-V supply, and the overall electric consumption to move a heliostat is about 2 W, which means that the electric power required per reflective surface unit is 24 W/m^2.

Each stepper motor has its own driver, while a processing unit and an electronic routing device indicate the number of steps that each of the 180 stepper motors has to move to track the sun's apparent motion. The tracking system currently has an open-loop control, so it is very important to calibrate the heliostats' position precisely to ensure a good tracking accuracy. The open-loop strategy can introduce a significant positioning error by comparison with the closed-loop control [28], but no positioning feedback was foreseen in our prototype plant for the sake of simplicity and to contain the costs. The heliostat starts to move from a well-known, mechanically defined position. Once the final position needed to focus the solar radiation on the focal point is defined, it is possible to calculate the two tracking angles, and thus the steps that each motor has to make.

3. THEORETICAL SIMULATION OF THE CONCENTRATOR'S PERFORMANCE

A theoretical study of the distribution of the light on the receiver was conducted with the aid of a computer simulation program, using a sunbeam tracing technique to model the sunlight's reflection by the heliostat concentrator, and to plot the distribution of the solar flux distribution on the target plane. To calculate the effective amount of reflected radiation incident on the receiver with a reasonably high resolution, each tilted mirror was divided into a matrix of squares, S_{kl}, each of which was 1 cm^2 in size. For each square, the coordinates of the center of mass, G_{kl}, and its minimum normal distance from the receiver were calculated. It proved necessary to define the equation for the plane of the receiver, which can be set horizontal to the ground or tilted on the x-axis (γ). The equation for the plane π of the focal area is as follows:

$$\mathrm{a} = 0 \tag{11}$$

$$\mathrm{b} = \sin(\gamma) \tag{12}$$

$$\mathrm{c} = -\cos(\gamma) \tag{13}$$

$$\mathrm{q} = |\mathrm{x_F}\cdot\mathrm{a} + \mathrm{y_F}\cdot\mathrm{b} + \mathrm{z_F}\cdot\mathrm{c}| \tag{14}$$

The dimension of the target plane can be varied to suit the application considered and its purposes. In this study, a circular shape was adopted for the focal area, and two different diameters were considered to assess the effect of diameter on the optical efficiency and the concentration ratio achievable, that is, (i) $diam = 400$ mm, which was found to maximize optical efficiency, and (ii) $diam = 250$ mm, which afforded a greater homogeneity and concentration.

By applying the mirror-to-receiver vector to the center of mass of the small reflecting area, it is possible to determine where the reflected beam hits the receiver plane. The coordinates of the point Gr_{kl}, where the beam hits the focal plane, are as follows:

$$Gr_{kl} = \begin{bmatrix} x_{Gr,kl} \\ y_{Gr,kl} \\ z_{Gr,kl} \end{bmatrix}_{kl} = \begin{bmatrix} x_G + d_{G-\pi,kl}\cdot r_{x,kl} \\ y_G + d_{G-\pi,kl}\cdot r_{y,kl} \\ z_G + d_{G-\pi,kl}\cdot r_{z,kl} \end{bmatrix}_{kl} \tag{15}$$

where $d_{G-\pi,kl}$ is the distance between the central point of the small reflecting area, with the coordinates x_G, y_G, z_G, and the focal plane:

$$d_{G-\pi,kl} = \frac{-q - a\cdot x_{G,kl} - b\cdot y_{G,kl} - c\cdot z_{G,kl}}{a\cdot r_{x,kl} + b\cdot r_{y,kl} + c\cdot r_{z,kl}} \tag{16}$$

The solar radiation conveyed by the reflecting square area is only counted if the reflected beam hits the receiver inside a circle, the diameter, $diam$, of which is centered around the focal point. This happens when

$$d_{Gr-F,kl} = \sqrt[2]{\left(x_{Gr,ij} - x_F\right)^2 + \left(y_{Gr,ij} - y_F\right)^2 + \left(z_{Gr,ij} - z_F\right)^2} < (diam/2) \tag{17}$$

Power intensity maps over the focal plane can be calculated, depending on the density of the rays hitting the plane. The cosine effect is taken into account because the mirrors are not perpendicular to the solar unit vector. The scalar product of the sun vector and the bisector vector (normal to the mirror) gives the cosine of the angle.

$$\cos(\beta) = \vec{s}\cdot\vec{n} = \vec{n}\cdot\vec{r} \tag{18}$$

This must be multiplied by the area of the square, S_{kl} , to assess the effective active surface of the mirror correctly. The available reflecting surface of each reflecting area $S_{u,kl}$ can be calculated as

$$S_{u,kl} = S_{kl}\cos(\beta) \tag{19}$$

so the available surface for each mirror can be calculated as

$$S_{u,ij} = \sum_k \sum_l S_{u,kl} \tag{20}$$

and the total available surface of the concentrator is consequently

$$S_{u,tot} = \sum_i \sum_j S_{u,ij} \tag{21}$$

The solar concentration ratio on the focal plane is essentially a measure of how many times the solar radiation is concentrated over the receiver by comparison with the total useful reflective surface. The calculation of the solar

concentration ratio (number of suns) can thus be described as

$$C = \frac{\int_{S_{rec}} I_r \, dS_{rec}}{S_{rec} \cdot DNI} = \frac{S_{u,tot}}{S_{rec}} \tag{22}$$

where I_r is the flux distribution on the area of the receiver, DNI is the direct normal irradiance, and S_{rec} is the area of the receiver on the focal plane.

Another result that can be obtained is the optical efficiency of the system, which can be calculated as

$$\eta_{opt} = \frac{S_{u,tot}}{S_{tot,ref}} \tag{23}$$

where $S_{tot,ref}$ is the total reflective area of the mirrors.

3.1. Implementing the tracking error algorithm

Even if the ideal concentration ratio can be calculated very accurately, it is impossible to guarantee a perfect mechanical mounting and perfectly reliable tracking. Because different kinds of error can occur, it is difficult to consider and quantify them all. Mounting errors due to the heliostats being positioned wrongly cause a displacement of the resulting mirror image on the focal plane. It is rare for such mounting position errors to run to several millimeters because it is quite easy to achieve a good positioning precision. In any case, the image's displacement would be exactly the same as the mounting error, so the latter would have only a minimal effect in the application considered here.

An error in the tracking angle could have a much worse influence on the concentrator's performance, as reported in an analytical study by Badescu [29]. In fact, the heliostats' tracking angles are crucial to the system's focusing capabilities, as much as other inaccuracies such as the mirrors' planarity errors and the sunshape [30,31]. For this reason, a pointing error is always assumed in the heliostat angles θ_{ij} and α_{ij}. To take this kind of tracking angle mismatch into account, a randomly distributed error is added to, or subtracted from the ideal value. In the present study, a beta distribution (with the parameters $\alpha = 2$ and $\beta = 4$) was used to define a random error in the range of ±1° with a mean of 0.33° (5.76 mrad) and a mode of 0.25° (or 4.36 mrad). If this beta distribution is compared with the error distribution probability function reported in [29], it is slightly more conservative as there is a bigger probability that higher tracking errors occur (see next section for a more detailed comparison). The reported mean alignment error value errs on the side of caution; that is, it is particularly high if compared with the accuracy achievable with existing heliostat plants. In such plants, the maximum pointing error can be kept below 3–4 mrad, while the mean error is generally less than 2–2.5 mrad if accurate tracking calibration methods are used [32,33]. In addition, the small size of our plant and the consequently short distance of the focal plane from the mirror reduce the effect of any angular positioning error on the position of the mirror's image on the focal plane.

Once the tracking errors ε_θ and ε_α (elevation and azimuth error) have been calculated, we can define the new tracking angles as follows:

$$\theta_{e,ij} = \theta_{ij} + \varepsilon_{\theta,ij} \tag{24}$$

$$\alpha_{e,ij} = \alpha_{ij} \, \varepsilon_{\alpha,ij} \tag{25}$$

The mean tracking error of a heliostat used in the concentrator can be evaluated as follows:

$$\varepsilon_{i,j} = \sqrt{\varepsilon_{\theta,ij}^2 + \varepsilon_{a,ij}^2} \tag{26}$$

The components of the unit vector $\rightarrow n_{ij}$ describing the normal to the mirror are

$$\vec{n}_{ij} = \begin{bmatrix} n_{xe,ij} \\ n_{ye,ij} \\ n_{ze,ij} \end{bmatrix}_{ij} = \begin{bmatrix} cos(\theta_{e,ij}) cos(\alpha_{e,ij}) \\ cos(\theta_{e,ij}) sin(\alpha_{e,ij}) \\ sin(\theta_{e,ij}) \end{bmatrix}_{ij} \tag{27}$$

The new reflected sunbeam $\vec{r}_{e,ij}$, which includes the tracking error, can be calculated as:

$$\vec{r}_{e,ij} = 2 \, \vec{n}_{e,ij} (\vec{s} \cdot \vec{n}_{e,ij}) + \vec{s} \tag{28}$$

The unit vector $\vec{r}_{e,ij}$ can now be applied to each of the square reflective elements to determine the point where the reflected beam hits the focal plane.

4. RESULTS AND DISCUSSION

In this section, the main results of the simulations from the ray-tracing algorithm are presented. The first aim of the simulation was to identify the best geometrical configuration of the concentrator in order to achieve the maximum optical efficiency (calculated according to Eq. (23)) with varying the position of the receiver and of the mirrors' plane.

Regarding the position of the receiver, its height from the ground can be varied; thus, the position of the focal plane on the z-axis can be regulated; the position over the x-axis and the y-axis is kept constant (the x-axis position is located in the center of the mirror's field, $x = 1990$ mm, as well as the y-axis position, $y = 1000$ mm). Figure 2 shows the trend of the concentrator's optical efficiency as a function of the height of the focal point above the ground. Shortening the focal distance reduces the efficiency of the system: the cosine losses increase, and the image of the mirrors on the focal plane suffers from more severe aberration effects. On the other hand, when the focal point is too far from the heliostats, the effect of the tracking angle errors leads to a dispersion of the mirrors' images on the focal plane, so the light spot is larger than the receiver's aperture and the system's optical efficiency deteriorates. An optimal height for the focal point was found at about $z = 4000$ mm, where both cosine losses and tracking error

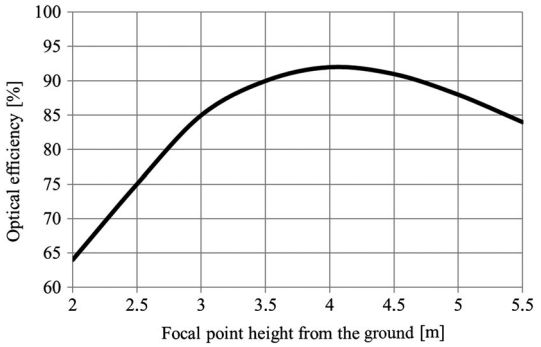

Figure 2. Effect of the focal point's distance from the mirrors on the optical efficiency.

losses are minimized and the distance-to-tower-height ratio of the farther heliostat is kept lower than 0.5.

As far as the position of the heliostats is concerned, it is possible to vary the tilt angle of the mirrors plane by rotating it over the *x*-axis. In Figure 3, the influence of the tilt angle of the mirrors' plane on the optical efficiency of the concentrator is reported. In the summer period at solar noon, the optical efficiency has a peak when the plane is tilted by 20°, while during the winter solstice, the efficiency is slightly better when the plane is tilted by 25°. The same behavior can be recorded early in the morning at 8 AM, even though the efficiency curve is shifted to lower values because of the higher blocking and shadowing losses. Table I reports the combination of the shadowing and the blocking losses depending on the tilt angle of the heliostat plane. The losses are reduced when the heliostat plane has a higher tilt angle; when the tilt angle is 25°, the yearly average losses are about 7.5%, which is only slightly higher than traditional large-scale plant, but with a much higher packing factor. William and Micheal [34] report a yearly averaged value of the shadowing and blocking losses of about 5.6% for a typical central tower plant. Using the same procedure, Table II reports the average cosine losses of the heliostats vs tilt angle. In this case, the losses increase with higher tilt angle of the plane because the height of the heliostats placed more northern is higher and the distance-to-height ratio is increased, which reflects in a worse solar beam incidence angle. Nevertheless the values of the cosine losses are significantly lower than for large-scale plants, thanks to the very low distance of the heliostats from the receiver. A typical heliostat concentrator has a yearly averaged cosine loss of 23.6% as reported in [34]. On the basis of the aforementioned results, considering the overall annual optical efficiency, it is possible to conclude that the best trade-off of the losses is obtained when the mirrors' plane is tilted by about 20° over the *x*-axis for the considered installation.

Table III reports the overall optical efficiency of the concentrator in different hours and periods of the year. These values take into account the blocking and the shadowing losses as well as the cosine losses. The annual average field optical efficiency of the concentrator, which

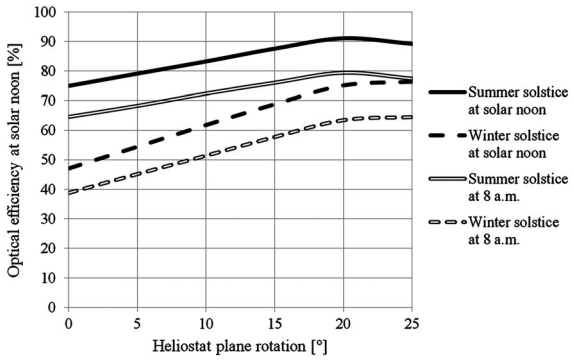

Figure 3. Dependence of the optical efficiency on the tilt angle of the heliostats' plane.

Table II. Cosine losses of the concentrator in different periods of the year and with varying the heliostat plane tilt angle.

	Cosine losses				
Heliostat plane tilt angle	21 of December 8 AM (%)	21 of December 12 AM (%)	21 of June 8 AM (%)	21 of June 12 AM (%)	Yearly average cosine losses (%)
0°	24.9	14.2	12.6	2.5	12.5
5°	25.2	14.5	12.7	2.7	12.7
10°	25.4	14.7	12.8	2.9	12.9
15°	25.7	15.0	13.0	3.1	13.2
20°	26.1	15.6	13.1	3.4	13.5
25°	26.6	16.1	13.1	3.6	13.9

Table I. Blocking and shadowing losses of the concentrator in different periods of the year and with varying the heliostat plane tilt angle.

Heliostat planetilt angle	21 of December 8 AM (%)	21 of December 12 AM (%)	21 of June 8 AM (%)	21 of June 12 AM (%)	Yearly average shadowing and blocking losses (%)
0°	47.2	33.9	25.0	17.7	27.9
5°	38.3	25.0	20.4	13.1	22.0
10°	29.4	21.1	15.8	10.5	17.0
15°	20.6	15.3	11.2	6.9	13.1
20°	12.3	9.0	7.2	3.9	7.8
25°	10.1	6.8	7.3	3.8	7.5

Table III. Overall optical efficiency of the concentrator in different periods of the year.

	Overall optical efficiency				
	8 AM (%)	10 AM (%)	12 PM (%)	2 PM (%)	4 PM (%)
Summer solstice	79.3	87.2	91.1	87.4	79.4
Winter solstice	63.5	71.4	75.0	70.9	62.3

also considers the reflectivity of the mirrors, is evaluated in 67.73% that is a higher value than the traditional large-scale central receiver plants. About the latter, William and Micheal [34] reported an optical efficiency of about 55%; a technical report from the National Renewable Energy Laboratory [35] indicates an overall field optical efficiency of 57%, while a study on the optimization of the heliostat layout by Collado and Guallard [36] calculates a maximum optical efficiency that ranges between 55% and 60% depending on the receiver dimension and the tower height.

Given the geometrical conditions that showed the best overall optical efficiency ($x = 1990$ mm, $y = 1000$ mm, $z = 4000$ mm, and the heliostat frame rotated through 20° around the x-axis), it is possible to describe the main results obtained by the simulation using the ray-tracing technique.

Figure 4 shows the comparison of the cosine efficiency of the concentrator at 8 AM in the summer and winter solstice. The coordinate reference system is centered on the focal point, and the distance of the heliostats from the receiver is reported in terms of 'tower heights' which, in the described plant, is 4000 mm over the soil. As expected, the heliostats placed westward have lower cosine losses both in summer and in winter period because of the smaller angle of incidence of the solar rays on the heliostat to reflect the solar radiation to the receiver. Figure 5 reports the cosine efficiency at 12 PM in the same periods of the year. It is possible to notice how the cosine losses are significantly reduced if compared with traditional large-scale central receiver plants.

By means of the ray-tracing technique, it is possible to evaluate the distribution of the reflected rays over the receiver taking into account the cosine losses and the distortion of the heliostat image over the receiver. In almost all the working conditions, most of the reflected rays are inside a circle with a radius of 300 mm. Figure 6 shows the flux distribution at noon on June 21st: the flux distribution profile has a bell shape with a peak of concentration in the

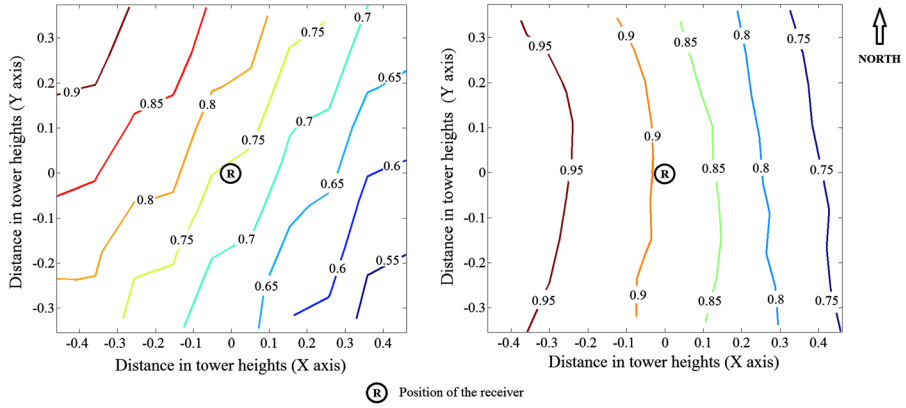

Figure 4. Cosine efficiency of the concentrator in winter and summer solstice at 8 AM.

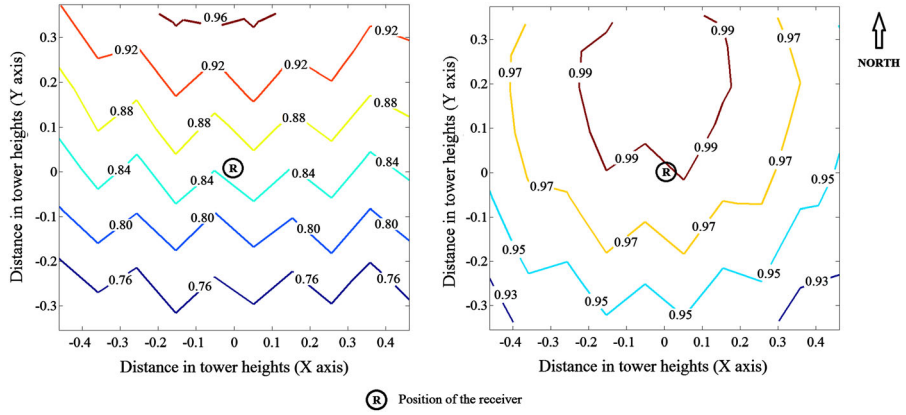

Figure 5. Cosine efficiency of the concentrator in winter and summer solstice at 12 PM.

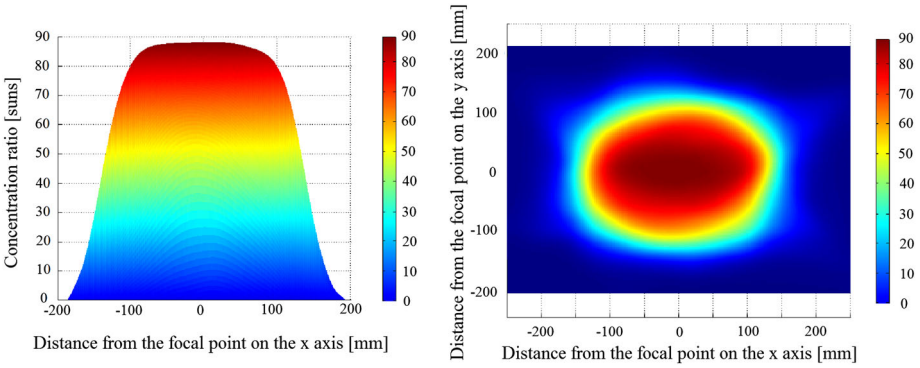

Figure 6. Flux distribution, in suns, over the focal plane on 21 June (mid-day).

focal point. In summer, the concentration ratio in the focal point reaches 88 suns and has a homogeneous distribution over the receiver. The flux distribution was evaluated also in winter when the peak concentration is lower: it reaches 85 suns, but a steep drop of the concentration is registered just few millimeters far from the focal point, so that the overall concentration ratio is reduced.

As mentioned, the concentration ratio calculated using Eq. (22) depends on the size of the target plane. The solar concentration over a receiver with 250 mm aperture and 400 mm aperture is shown in Figure 7 for the solstice days; in summer, the concentration ratio touches almost 80 suns. The trend reported in Figure 7 reflects the effect of all the optical losses of the concentrator: because these losses are lower in the central hours of the day, the concentration ratio is higher. If the receiver's aperture is increased to a diameter of 400 mm, the concentration ratio is reduced (50 suns on the summer solstice) because the outer part of the receiver is hit by a less intense reflected solar radiation as shown in Figure 6.

The opposite trend is recorded for the optical efficiency (described by Eq. (23)) on varying the receiver's aperture. Figure 8 shows the optical efficiency of the system for the winter and summer solstice days. With a receiver aperture of 250 mm, the efficiency reaches a peak of 58% on 21 June and 52% on 21 December, while using a receiver with an aperture of 400 mm, a peak optical efficiency of over 91% is reached for the summer solstice and 76% for the winter solstice.

The total power on the focal plane can be evaluated when the total available surface area $S_{u,tot}$ is known. The values of direct normal irradiance (DNI) used to evaluate the power on the receiver were obtained from the Bird's clear sky model [37] for a typical bright sunny day in the center of Italy; the peak value reaches 906 W/m^2 at mid-day on 21 June. The total power over the receiver is

$$R_{tot} = S_{u,tot} DNI_{ref} \eta_{mir} \tag{29}$$

where η_{mir} is the reflectivity of the mirrors used for the heliostats. A study by Fend *et al.* [38] considered a value of 90% as a plausible reflectivity index for most of the mirrors used for solar concentration purposes, over the whole solar light spectrum. The available power over a receiver with a 400-mm aperture is represented in Figure 9, while a receiver with an aperture of 250 mm obviously shows a lower amount of power. In these figures, the value of the power available at the receiver reflects the trend of the optical efficiency and the trend of the available DNI,

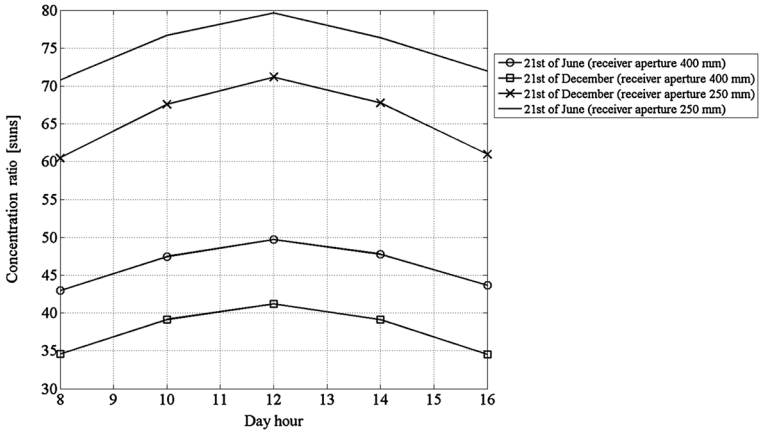

Figure 7. Solar concentration ratio over a solar receiver.

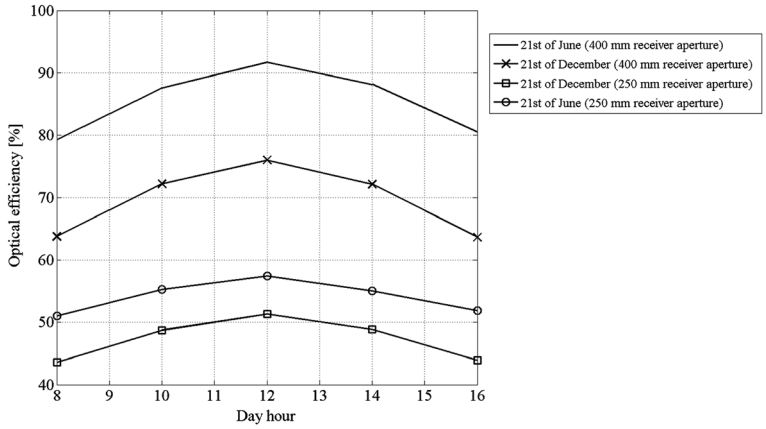

Figure 8. Optical efficiency of the plant over a solar receiver.

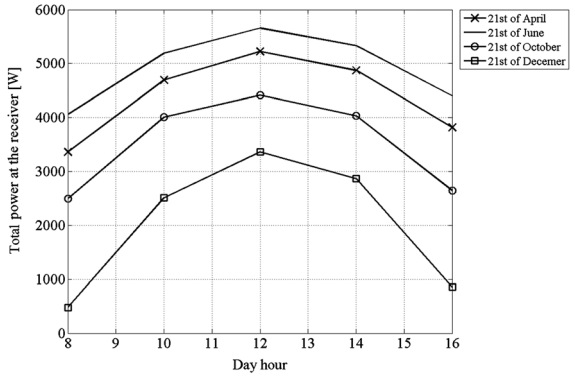

Figure 9. Total power over the focal plane for a solar receiver with a 400-mm aperture.

which are both higher in the central hours of the day and in summer period. Over a 400-mm aperture receiver, the total power has a peak of over 5700 W in summer and 3300 W in winter; a receiver with an aperture of 250 mm has a peak of power of 3500 W in summer and 2300 W in the winter solstice. This means that the necessary collector aperture ranges between 1.3 and 2.1 m^2/kW_{max}.

According to this simulated result and the achievable solar concentration, theoretical maximum temperature on the receiver can be calculated using the black body radiation equation:

$$T_{\max} = \sqrt[4]{\frac{C\ DNI_{ref}\ \ \eta_{mir}}{\sigma_s}} \tag{30}$$

where (σ_s) is Stefan–Boltzmann constant. Considering a direct solar irradiance DNI_{ref} of 900 Wm^{-2}, the maximum achievable temperature, neglecting the thermal losses, is 646 °C for the 400-mm aperture receiver and 760 °C for the 250-mm aperture receiver.

Eventually, the results of the simulations show that a very good optical efficiency can be achieved with the heliostat system described here, even in the event of sizable tracking errors (a random distribution error was adopted with a mode of ±0.25° [4.36 mrad], as explained in Section 3.1). Figure 10 shows the trend of the optical efficiency as a function of the mean tracking angle error of the 180 stepper motors at the solar noon in winter and summer solstice. The maximum optical efficiency drops slightly as long as the error was kept below 5 mrad. When the mean tracking error is greater, the optical efficiency deteriorates more sensibly. In Figure 16, a comparison with the error distribution reported in [29] is also provided: the optical efficiency trends are similar, but a smaller reduction of the optical efficiency for higher values of the tracking error is obtained when the error distribution in [27] is adopted. This confirms that our choice of the error β distribution is reasonable and conservative.

4.1. Possible applications

In this section, possible applications of the aforementioned CSP system are presented, with particular focus on small-scale and building integration applications. Because no secondary optics is used in this system, the concentration ratio does not reach very high levels; anyway, medium concentration ratios are still suitable for many applications, such as low temperature power generation [39–41], industrial process heat [42,43], solar cooling [44–46], and methanol reforming for hydrogen production [47].

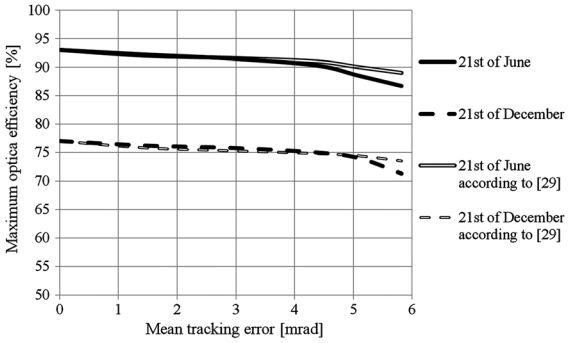

Figure 10. Dependence of optical efficiency on mean tracking error.

As far as power generation is concerned, when the solar concentrator is coupled with organic rankine cycles (ORC), temperature lower than 150 °C are necessary. Delgado-Torres and Garcia-Rodriguez [39] presented an analysis of low temperature solar ORC cycles using different commercial solar concentrators and, for example, for a parabolic collector, an aperture area of about 23 m^2 for every kilowatt of net power produced is requested, that means 2.3 m^2 for kilowatt provided to the receiver by the collector considering a power cycle efficiency of 10%. Such a value is in accordance with those for our concentrator.

Similarly, for solar cooling applications, a temperature lower than 100 °C is required by single effect chillers, while higher values are necessary for double-stage absorption units [42]. Chemisana *et al*. [44] stated that a temperature around 150 °C has to be achieved by solar concentrators coupled with double effect absorption chillers. They consider systems that can obtain a concentration ratio in the range of 10–20 with simple configurations to be easily integrated in the facade of buildings. A design value of about 5.4 m^2 for every kilowatt of cooling capacity is assessed, that is, 7.29 m^2 for kilowatt provided to the receiver by the collector (COP = 1.35). Much lower collector surface is necessary with our concentrator that can achieve a higher concentration ratio.

Comparing the proposed concentrator with other traditional systems for the production of thermal power for industrial or residential applications, such as parabolic trough, it is evident that the latter are generally simpler devices, with slightly lower costs and comparable concentration ratio [48,49]. On the contrary, the small-scale heliostat concentrator has the advantage of a better optical efficiency and an easier installation, especially for the integration on vertical facades or on rooftops. Another competitive technology in the production of thermal power for building energy demand is the coupling of traditional PV systems with heat pumps. Even in this case, the proposed heliostat seems to be competitive: considering the overall occupied area of 7.5 m^2, which corresponds to an electric power production of about 1 kW_e by PV panels, also with a performing heat pump, the maximum deliverable thermal power would be about 4 kW_{th}, while our concentrator can produce up to 5.5 kW_{th}. Taking into account the different thermal power deliverable and the total cost of the two systems (heliostat concentrator versus PV panels + heat pump), the small-scale heliostat concentrator can be considered economically feasible. In addition, much higher temperature than a heat pump or a traditional solar panel can be reached.

Concentration PVs are another potential application of the heliostat, but further studies are needed to assess the effect of an uneven light intensity distribution on the PV cell.

Concluding, a brief analysis of the total cost for the realization of the concentrator is reported. The parts considered for the design of the concentrator are off-the-shelf components that can be easily found and bought at a competitive price. Table IV reports the breakdown of the cost of the most significant items. The overall cost of a system with 90 mirrors is about €3.650, with the tracking stepper motors being the most costly item. The receiver of the solar radiation is not considered in this evaluation because the characteristics of the heat exchanger depend on the application and on the cooling fluid used; anyway, the complexity and the cost of the receiver are limited when the involved working temperatures are not too high, as for the aforementioned technologies.

Table IV. Cost of the main items of the solar concentrator.

Component	Quantity	Unity cost (€)	Total cost (€)
Receiver structure	1	470.00	470.00
Heliostats' plane chassis	1	280.00	280.00
Electronic PCB and stepper motor driver	1	450.00	450.00
Electric stepper motors	180	8.00	1440.00
Heliostats' tracking mechanism	180	2.61	469.80
Mirror mount and reflective material	7.5 m^2	47.34	355.05
Stepper motor wiring and protection	180	0.85	153.00
Total			3617.85

PCB, printed circuit board.

It is worth noting that the prices considered in this evaluation refer to the component cost for the production of a single prototype; much lower expenditure could be achieved with the advantage of economies of scale in an industrial production. In particular, the cost of the tracking stepper motors and the electronic printed circuit board could be consistently reduced. It is possible to forecast a reduction of the overall cost up to about €2400 per unit, which means about €420/kW_{th}. Even though this goal could be accomplished, the electric power production by means of the presented concentrator is not comparable from the economic point of view with the present electricity cost by silicon PV panels [50]. On the other hand for thermal applications (heating, solar cooling, and process heat), the cost performance of such a small-scale CSP system can be competitive against other concentration and traditional solutions [48,49], also considering the further improvements achievable with the ongoing development work.

5. CONCLUSIONS

This paper describes and analyzes the overall performance of a small-sized non-imaging focusing heliostat concentrator. A beam-tracking algorithm was used to simulate a prototype concentrator comprising 90 flat heliostats moved by a two-axis tracking mechanism. The results of the simulation confirmed that the flat-mirror heliostat concentrator can perform well in terms of optical efficiency, thanks mainly to the narrow gap between the heliostat and the receiver, which limits the influence of the tracking errors. Such a system can also

generate a reasonably uniform solar irradiance at the focal plane, especially if the receiver's aperture is limited to 250 mm in diameter. It is worth noting that reasonable tracking errors were taken into account in the simulation of the concentrator, so the reported performance refers to realistic working conditions. The concentration ratio over the receiver reached a maximum of 80 suns using an aperture of 250 mm and 50 suns with an aperture of 400 mm. In the latter case, the optical efficiency is very high throughout the day and peaked at 91% at mid-day on 21 June. Eventually, the performance and cost analysis of such small-scale CSP system showed low competitiveness about electricity production, while interesting thermal applications in comparison with traditional solutions.

NOMENCLATURE

a, b, c, q	= coefficients of the equation of the focal plane
C	= concentration ratio
d	= distance [mm]
$diam$	= diameter of the circular focal area [mm]
DNI	= value of direct normal irradiance [W/m^2]
F	= focal point
G	= central point of square reflecting area
Gr	= point on the focal plane hit by the reflected ray
h	= height of the hexagonal mirror [mm]
h_z	= height off the ground of the mirror's plane [mm]
l	= diagonal of the hexagonal mirror [mm]
m	= max number of concentrator columns
n	= max number of concentrator rows
$\vec{\mathrm{n}}$	= normal unit vector
$\vec{\mathrm{N}}$	= normal vector
P	= central point of mirror
Pr	= central point of rotated mirror
res	= column position correction parameter
$\vec{\mathrm{r}}$	= unit vector pointing to the focal point
$\vec{\mathrm{s}}$	= solar unit vector
S	= area [mm^2]
x, y, z	= coordinates in the Cartesian reference system [mm]
R	= power over the receiver aperture [W]

Greek symbols

α	= azimuth angle [grad]
β	= cosine effect angle [grad]
ε	= Tracking error [grad]
ϕ	= angle of rotation of the mirror's plane [grad]
γ	= tilt angle of the focal plane over the x-axis [grad]
η	= efficiency
π	= focal plane
θ	= zenith angle [grad]

Subscripts

e	= error
F	= focal point
G	= central point of square reflecting area
Gr	= point on the focal plane hit by the reflected ray
i	= mirror row number
j	= mirror column number
k	= square reflecting surface row number
l	= square reflecting surface column number
mir	= mirror
opt	= optical
P	= mirror central point
Pr	= central point of rotated mirror
s	= solar
rec	= receiver
ref	= reflective
tot	= total
u	= useful
x, y, z	= coordinates in the Cartesian reference system [mm]
α	= azimuthal
θ	= zenithal

REFERENCES

1. International Energy Agency (IEA). Energy technology prospective, 2008.
2. International Energy Agency (IEA). Technology roadmap: concentrating solar power, 2010.
3. Vallentin D, Viebahn P. Economic opportunities resulting from a global deployment of concentrated solar power (CSP) technologies — the example of German technology providers. *Energy Policy* 2010; **38**:4467–4478.
4. Yan Q, Hu E, Yang Y, Zhai R. Evaluation of solar aided thermal power generation with various power plants. *International Journal Of Energy Research* 2011; **35**:909–922.
5. European Renewable Energy Council (EREC). Energy revolution, 2007.
6. Rawlins J, Ashcroft M. Small-scale concentrated solar power. A review of current activity and potential to accelerate deployment, Department of Energy and Climate Change, UK, 2013.
7. Zamfirescu C, Dincer I, Stern M, Wagar WR. Exergetic, environmental and economic analyses of small-capacity concentrated solar-driven heat engines

for power and heat cogeneration. *International Journal Of Energy Research* 2012; **36**:397–408.
8. Rohr B. The promise of small heliostats, Northeast Sun, 2009; 7–12.
9. Pikra G, Salim A, Prawara B, Purwanto AJ, Admona T, Eddy Z. Development of small scale concentrated solar power plant using organic Rankine cycle for isolated region in Indonesia. *Energy Procedia* 2013; **32**:122–128.
10. Neber M, Lee H. Design of a high temperature cavity receiver for residential scale concentrated solar power. *Energy* 2012; **47**:481–487.
11. Barlev D, Vidu R, Stroeve P. Innovation in concentrated solar power. *Solar Energy Material and Solar Cells* 2011; **95**:2703–2725.
12. Chen YT, Chong KK, Bligh TP, Chen LC, Yunus J, Kannan KS, Lim BH, Lim CS, Alias MA, Bidin N, Aliman O, Salehan S, Rezan SA, Tam CM, Tan KK. Non-imaging focusing heliostat. *Solar Energy* 2001; **73**:155–164.
13. Chen YT, Chong KK, Lim CS, Lim BH, Tan KK, Aliman O, Bligh TP, Tan BK, Ismail G. Report of the first prototype of non-imaging focusing heliostat and its application in high temperature solar furnace. *Solar Energy* 2002; **72**:531–544.
14. Chen YT, Chong KK, Lim BH, Lim CS. Study of residual aberration for non-imaging focusing heliostat. *Solar Energy Materials and Solar Cells* 2003; **79**:1–20.
15. Chen YT, Chong KK, Lim CS, Tan BK, Lim BH, Lu YF. Report on the second prototype of non-imaging focusing heliostat. *Solar Energy* 2005; **79**:280–289.
16. Chong KK. Optical analysis for simplified astigmatic correction of non-imaging focusing heliostat. *Solar Energy* 2010; **84**:1356–1365.
17. Chong KK, Lim CY, Hiew CW. Cost effective solar furnace system using fixed geometry non-imaging focusing heliostat and secondary parabolic concentrator. *Renewable Energy* 2011; **36**:1595–1602.
18. Danielli A, Yatir Y, Mor O. Improving the optical efficiency of a concentrated solar power field using a concatenated micro-tower configuration. *Solar Energy* 2011; **85**:931–937.
19. Schramek P, Mills DR. Multi-tower solar array. *Solar Energy* 2003; **75**:249–260.
20. Winston R, Minano JC, Benitez P. *Non-imaging Optics*. Elsevier Academic Press: New York, 2005; 1–6.
21. Blanco-Muriel M. Alarcon Padilla DC, Lopez Moratalla T, Lara-Coira M, Computing the solar vector. *Solar Energy* 2001; **70**:431–441.
22. Michalsky JJ. The Astronomical Almanac's algorithm for previous approximate solar position (1950–2050). *Solar Energy* 1988; **40**:227–235.
23. Di Buò G, Ippoliti G, Renzi M, Pirro M, Longhi S, Sileoni S. CSP control system implementation on embedded board, International Conference on Clean Electrical Power Renewable Energy Resources Impact, 2013.
24. Kolb GJ, Jones SA, Donnelly MW, Gorman D, Thomas R, Davenport R, Lumia R. Heliostat Cost Reduction Study, Sandia Report, SAND2007-3293, 2007.
25. Sanchez M, Romero M. Methodology for generation of heliostat field layout in central receiver systems based on yearly normalized energy surfaces. *Solar Energy* 2006; **80**:861–874.
26. Wei X, Lu Z, Yu W, Wang Z. A new code for the design and analysis of the heliostat field layout for power tower system. *Solar Energy* 2010; **84**:865–890.
27. Noone CJ, Torrilhon M, Mitsos A. Heliostat field optimization: a new computationally efficient model and biomimetic layout. *Solar Energy* 2012; **86**:792–803.
28. Kribus A, Vishnevetsky I, Yogev A, Rubinov T. Closed loop control of heliostats. *Energy* 2004; **29**:905–913.
29. Badescu V. Theoretical derivation of heliostat tracking errors distribution. *Solar Energy* 2008; **82**:1192–1197.
30. Collado FJ. Quick evaluation of the annual heliostat field efficiency. *Solar Energy* 2008; **82**:379–384.
31. Stone KW, Lones SA. Analysis of solar two heliostat tracking error sources; Sandia National Laboratory internal document, 1999.
32. Collado FJ. One-point fitting of the flux density produced by a heliostat. *Solar Energy* 2010; **84**:673–684.
33. Weidong H, Huairui L, Longlong L, Peng H, Zeshao C. Gauss–Legendre integration of an analytical function to calculate the optical efficiency of a heliostat. *Solar Energy* 2013; **92**:7–14.
34. William BS, Micheal G. Power from the sun, 2001. Available from: http://www.powerfromthesun.net/book.html. Accessed on June 2014.
35. NREL technical monitor, Assessment of Parabolic Trough and Power Tower Solar Technology Cost and Performance Forecasts, NREL/SR-550-34440, 2003.
36. Collado FJ, Guallar J. A review of optimized design layouts for solar power tower plants with campo code. *Renewable and Sustainable Energy Reviews* 2013; **20**:142–154.
37. Bird RE, Hulstrom RL. A simplified clear sky model for direct and diffuse insolation on horizontal surfaces, Solar Energy Research Institute, SERI/TR-642-761, 1981.
38. Fend T, Hoffschmidt B, Jorgensen GJ, Kuster H, Kruger D, Pitz-Paal R, Rietbrock P, Riffelmann KJ. Comparative assessment of solar concentrator materials. *Solar Energy* 2003; **74**:149–155.

39. Delgado-Torres AM, Garcia-Rodriguez L. Analysis and optimization of the low-temperature solar organic Rankine cycle (ORC). *Energy Conversion and Management* 2010; **51**:2846–2856.
40. Gang P, Jing L, Jie J. Design and analysis of a novel low-temperature solar thermal electric system with two-stage collectors and heat storage units. *Renewable Energy* 2011; **36**:2324–2333.
41. Pehlivantürk C, Özkan O, Baker DK. Modeling and simulations of a micro solar power system. *International Journal of Energy Research* 2013, In press. DOI: 10.1002/er.3119
42. Soteris AK. Solar thermal collectors and applications. *Progress in Energy and Combustion Science* 2004; **30**:231–295.
43. Fernandez-Garcia A, Zarza E, Valenzuela L, Perez M. Parabolic-trough solar collectors and their applications. *Renewable and Sustainable Energy Reviews* 2010; **14**:1695–1721.
44. Chemisana D, Lopez-Villada J, Coronas A, Ignasi Rosell J, Lodi C. Building integration of concentrating systems for solar cooling applications. *Applied Thermal Engineering* 2013; **50**:1472–1479.
45. Lu ZS, Wang RZ, Xia ZZ, Lu XR, Yang CB, Mac YC, Mac GB. Study of a novel solar adsorption cooling system and a solar absorption cooling system with new CPC collectors. *Renewable Energy* 2013; **50**:299–306.
46. Hovsapian R, Vargas JVC, Ordonez JC, Krothapalli A, Parise JAR, Berndsen JC. Thermodynamic optimization of a solar system for cogeneration of water heating and absorption cooling. *International Journal of Energy Research* 2008; **32**(13):1210–1227.
47. Liu Q, Jin H, Hong H, Sui J, Ji J, Dang J. Performance analysis of a mid- and low-temperature solar receiver/reactor for hydrogen production with methanol steam reforming. *International Journal of Energy Research* 2011; **35**:52–60.
48. Cabrera FJ, Fernandez-Garcıa A, Silva RMP, Perez-Garcıa M. Use of parabolic trough solar collectors for solar refrigeration and air-conditioning applications. *Renewable and Sustainable Energy Reviews* 2013; **20**:103–118.
49. Turchi C, Mehos M, Ho CK, Kolb GJ. Current and future costs for parabolic trough and power tower systems in the US market, National Renewable Energy Laboratory (NREL), September 2010.
50. Feldman D, Barbose G, Margolis R, Wiser R, Darghouth N, Goodrich A. Photovoltaic (PV) pricing trends: historical, recent, and near-term projections, National Renewable Energy Laboratory (NREL), November 2012.